High Temperature Phase Transformations and Superprotonic Conductivity in  $Cs_2(HSeO_4)(H_2PO_4)$ 

Grace Xiong<sup>1</sup>, Ara Jo<sup>1,2</sup>, Louis S. Wang<sup>1</sup>, and Sossina M. Haile\*<sup>1,3</sup>

### **Abstract**

The compound Cs<sub>2</sub>(HSeO<sub>4</sub>)(H<sub>2</sub>PO<sub>4</sub>) is of interest due to its high conductivity in its superprotonic state. In the present work, in situ X-ray diffraction studies, simultaneous thermal analysis, and AC impedance spectroscopy, each performed under controlled value of steam partial pressure (pH<sub>2</sub>O), were carried out to elucidate the crystallographic features of the transformation and resolve the conductivity in the high temperature phase. The studies reveal that the material transforms to a cubic phase at a temperature of approximately 116 °C, that the activation energy for proton transport in the cubic phase is 0.304(2) eV, and the magnitude of the conductivity is comparable to that of Cs<sub>2</sub>(HSO<sub>4</sub>)(H<sub>2</sub>PO<sub>4</sub>). Despite differences in the room temperature structures of Cs<sub>2</sub>(HSeO<sub>4</sub>)(H<sub>2</sub>PO<sub>4</sub>), Cs<sub>2</sub>(HSO<sub>4</sub>)(H<sub>2</sub>PO<sub>4</sub>), and CsH<sub>2</sub>PO<sub>4</sub>, each has monoclinic to cubic transformation entropy of approximately 23 J/mol(CsH<sub>x</sub>XO<sub>4</sub>)/K. Under  $pH_2O = 0.05$  atm, the cubic phase of Cs<sub>2</sub>(HSeO<sub>4</sub>)(H<sub>2</sub>PO<sub>4</sub>) is stable to approximately 250 °C. Under elevated pH<sub>2</sub>O (0.3 atm), exsolution of a trigonal phase, with structure analogous to that of Cs<sub>3</sub>H(SeO<sub>4</sub>)<sub>2</sub>, was found to accompany the transformation to the cubic phase. While the driver for this transformation is not fully known, the cell volumes of both the exsolved and matrix phases indicate they are chemically distinct, respectively, from Cs<sub>3</sub>H(SeO<sub>4</sub>)<sub>2</sub> and Cs<sub>2</sub>(HSeO<sub>4</sub>)(H<sub>2</sub>PO<sub>4</sub>), suggesting additional chemical levers for control of transformation behavior.

**Keywords**: Superprotonic conductivity; phase transition; solid acid; non-stoichiometry; CsH<sub>2</sub>PO<sub>4</sub>

<sup>&</sup>lt;sup>1</sup>Department of Materials Science and Engineering, Northwestern University, Evanston, IL, 60208 USA

<sup>&</sup>lt;sup>2</sup>Present address: Department of Chemistry, Kangwon National University, Chuncheon 24341, Republic of Korea

<sup>&</sup>lt;sup>3</sup>Department of Chemistry, Northwestern University, Evanston, IL, 60208 USA

<sup>\*</sup>sossina.haile@northwestern.edu

### Introduction

Several oxyanion-bearing solid acids are described by an overall stoichiometry of M<sub>a</sub>H<sub>b</sub>(XO<sub>4</sub>)<sub>c</sub> where M is cation, typically an alkali species or NH<sub>4</sub>, and X is a group 5 or group 6 element that can be tetrahedrally coordinated by oxygen, such as P, S, Se or As. A subset of these compounds has a high-temperature superprotonic phase, in which the oxyanion group undergoes rapid reorientation and the hydrogen bond network linking the anion groups is highly disordered. Well-established examples include CsH<sub>2</sub>PO<sub>4</sub>,[1, 2] CsHSO<sub>4</sub>,[3-5] and Rb<sub>3</sub>H(SeO<sub>4</sub>)<sub>2.</sub>[6-8] Within this subset, several with stoichiometries in which the cation to oxyanion ratio is 1:1 adopt a cubic, CsCl-type structure in the superprotonic phase. Examples within this smaller group include the aforementioned CsH<sub>2</sub>PO<sub>4</sub>[1] and multi-anion compounds such as  $Cs_3(HSO_4)_2(H_2PO_4)$ , [9, 10]  $Cs_2(HSO_4)(H_2PO_4)$  [11] and  $Cs_5(HSO_4)_3(H_2PO_4)_2$ . [12, 13] Others with the 1:1 stoichiometry, such as CsHSO<sub>4</sub>[5] and CsHSeO<sub>4</sub>[3, 14] adopt a tetragonal scheelite-type structure in their respective superprotonic phases, whereas still others, such as Cs<sub>4</sub>(HSO<sub>4</sub>)<sub>3</sub>(H<sub>2</sub>PO<sub>4</sub>)[15] and Cs<sub>3</sub>(HSO<sub>4</sub>)<sub>2.5</sub>(H<sub>2</sub>PO<sub>4</sub>)<sub>0.5</sub>[12] enter into a mixed-phase region comprised of the cubic and tetragonal phases. The majority of proton conducting solid acid compounds with equimolar cation and anion contents adopt monoclinic structures at ambient temperatures. While most of these structures are distinct, they share a common feature of a globally ordered arrangement of hydrogen bonds. The transition to a phase with dynamically disordered hydrogen bonds induces an increase in conductivity by 3-5 orders of magnitude[16] and is often accompanied by a large heat of transformation, on the order of 9-12 kJ/mol (XO<sub>4</sub> unit).[1, 9, 13, 17]

The rich chemistry of oxyanion solid acids promises the possibility of continued discovery of new superprotonic compounds. Indeed, a number of compounds with chemistries similar to those with known superprotonic transitions have been reported in the literature and have yet to be fully characterized. Here we focus on Cs<sub>2</sub>(HSeO<sub>4</sub>)(H<sub>2</sub>PO<sub>4</sub>),[18] a compound that is chemically analogous to Cs<sub>2</sub>(HSO<sub>4</sub>)(H<sub>2</sub>PO<sub>4</sub>),[11, 17] but with a distinct structure at ambient temperature. As reported by Zouari et al. [18], differential thermal analysis, thermogravimetric analysis, and A.C. electrical impedance spectroscopy studies of Cs<sub>2</sub>(HSeO<sub>4</sub>)(H<sub>2</sub>PO<sub>4</sub>) suggest the occurrence of a polymorphic phase transition at 127 °C to a high-symmetry, superprotonic phase. Inspection of the high temperature diffraction pattern reported by Zouari et al. suggests the superprotonic phase to be cubic, however to date, the structure of that phase has not been solved.

Significantly, the conductivity reported by Zouari et al. for superprotonic Cs<sub>2</sub>(HSeO<sub>4</sub>)(H<sub>2</sub>PO<sub>4</sub>) is more than an order of magnitude lower than that reported for Cs<sub>2</sub>(HSO<sub>4</sub>)(H<sub>2</sub>PO<sub>4</sub>) [11] [19]. This result suggests a detrimental influence of the selenate chemistry on the overall transport behavior, which would be particularly surprising if the materials are isostructural. Accordingly, we undertook here a study of the high temperature phase of Cs<sub>2</sub>(HSeO<sub>4</sub>)(H<sub>2</sub>PO<sub>4</sub>) by high temperature in-situ X-ray powder diffraction, A.C. electrical impedance conductivity measurements, and thermal analysis.

#### Methods

The title compound was obtained by aqueous precipitation from a solution Cs<sub>2</sub>CO<sub>3</sub>, H<sub>2</sub>SeO<sub>4</sub>, and H<sub>3</sub>PO<sub>4</sub> in which the Cs<sub>2</sub>CO<sub>3</sub> concentration was slightly below that of a stoichiometric ratio of 1:1:1 for the three precursors. Precipitation was induced by gentle heating, with the solution held at 60 °C. Excess solution was removed from the product by rinsing with methanol. The resulting material was confirmed to be Cs<sub>2</sub>(HSeO<sub>4</sub>)(H<sub>2</sub>PO<sub>4</sub>) by X-ray powder diffraction (XRD), performed using a Rigaku Ultima IV diffractometer with a Cu source.

High temperature X-ray powder diffraction measurements were performed using a Smartlab 9 kW Gen 3 instrument (Cu Ka radiation,) equipped with an Anton Paar XRK 900 furnace used to both heat the sample and provide active humidification; pH<sub>2</sub>O conditions of 0.05 and 0.3 atm were studied. A relatively low power setting was used for the X-ray generator (40 kV, 20 mA) to avoid beam damage observed at more typical power settings. Powders were handground in a mortar and pestle for several minutes, then loosely packed into a spinning sample holder for the XRK furnace. High steam was introduced into the furnace at 110 °C, after collecting data at lower temperatures under dry (flowing N<sub>2</sub>) conditions. The temperature ramp under dry conditions was 10 °C/min between measurements, and the system was allowed to equilibrate for 10 min after reaching the target temperature prior to data collection. Steam was introduced for measurements under humidified conditions by flowing 30 sccm N2 through a water bubbler, held at 34 °C for 0.05 atm pH<sub>2</sub>O and at 70 °C for 0.3 atm pH<sub>2</sub>O. For reasons of convenience, slightly different heating profiles were used for the two steam conditions: under 0.05 atm, patterns were collected at 120, 125, and 130 °C, then at temperature intervals of 15 °C until 220 °C, using a heating rate of 2 °C/min between steps; under 0.3 atm, patterns were collected at 110, 130, 150, 170, and 200 °C using a heating rate of 10 °C/min between steps. In

both cases, after reaching the target temperature, the system was allowed to rest for 20 min prior to measurement. Diffraction patterns were analyzed using Rietveld refinement in GSAS-II[20]; the background, sample displacement, and lattice parameters of each phase were refined. The instrument profile parameters were obtained from measurement of a LaB<sub>6</sub> standard. The structural model of the monoclinic Cs<sub>2</sub>(HSeO<sub>4</sub>)(H<sub>2</sub>PO<sub>4</sub>) phase[18] was used for Rietveld analysis without refinement of atomic parameters. Additional parameters refined for the superprotonic phase are described in the discussion of its structure.

AC electrical impedance measurements were carried out using disc-shaped compacts of Cs<sub>2</sub>(HSeO<sub>4</sub>)(H<sub>2</sub>PO<sub>4</sub>) obtained by standard pressing procedures. The electrolyte material was ground to a fine powder and compressed in a uniaxial press under 98 kPa of pressure to obtain a final sample with >90% relative density,  $14.84 \pm 0.02$  mm in diameter, and  $1.14 \pm 0.02$  mm in thickness. Thin film platinum electrodes, 15 nm in thickness, were applied via sputtering using a Denton Desk Sputterer IV; Ag was found to react with Cs<sub>2</sub>(HSeO<sub>4</sub>)(H<sub>2</sub>PO<sub>4</sub>) under high temperature, high humidity conditions. The sample was electrically connected in a pseudo fourprobe configuration using silver wires (with the Pt film providing protection against reaction with the wires). Measurements were performed between 70 °C and 257 °C using a 4284A Agilent LCR analyzer, a voltage amplitude of 20 mV, and a frequency range of 1 Hz – 1 MHz. The heating rate was set at 5 °C/min and once the desired measurement temperature was reached, the sample was allowed to rest for 20 minutes prior to data collection. Between 85–120 °C measurements were performed under dry N<sub>2</sub> flow, with impedance spectra collected every 10-15 °C. At 120 °C, humidity ( $pH_2O = 0.05$  atm) was introduced through steam carried in N<sub>2</sub> (40 sccm) and measurements were then performed every 5 °C up to 220 °C. A slight (~ 15%) rise in conductivity was observed at 120 °C in response to the humidification, which is small relative to the many orders of magnitude increase that typically accompanies superprotonic phase transitions. Impedance data were analyzed using the ZView program.

Simultaneous thermogravimetric (TG) and differential scanning calorimetry (DSC) measurements were performed using a Netzsch STA (simultaneous thermal analyzer) 449 F3 under either dry flowing Ar, or humidified flowing Ar with  $pH_2O$  values of 0.04, 0.05, 0.2, and 0.4 atm, and a total gas flow rate of between 60–175 sccm, depending on the requirements for achieving the target  $pH_2O$ . Humidification was achieved using the integrated water vapor furnace of the STA. The Cs<sub>2</sub>(HSeO<sub>4</sub>)(H<sub>2</sub>PO<sub>4</sub>) samples, 40 mg in mass, were finely ground and

compacted into a Pt sample pan. For the experiment under dry Ar, the sample was heated at a constant rate of 1 °C/min to the maximum measurement temperature of 350 °C. For measurements under steam, the sample was first heated under dry Ar to a moderate temperature between 100 and 120 °C, at which point the steam was introduced and the system equilibrated for 1 h. At the lower humidification levels (0.04 and 0.05 atm  $pH_2O$ ) it was possible to lower the temperature to 80 °C for subsequent measurement without risk of steam condensation, and thus fully capture the features of the phase transition detected at ~ 120 °C without unusual features in the background. Following a brief equilibration at 80 °C, data were collected using a heating rate of 1 °C/min up to 275 °C. At the higher humidification levels (0.2 and 0.4 atm  $pH_2O$ ), aimed at establishing the dehydration behavior, data were collected from the initiation of humidification (110 and 120 °C, respectively) to 350 °C, again, using a heating rate of 1 °C/min.

### Results and Discussion

At room temperature, Figure 1, the structure of  $Cs_2(HSeO_4)(H_2PO_4)$  matches the monoclinic phase  $(P2_1/c)$  identified by Zouari.[18] The diffraction measurements under light humidification  $(pH_2O=0.05 \text{ atm})$  revealed the onset of a transition between 110 and 120 °C. Several peaks decrease in relative intensity (for example, a major peak at 22.5 °) between these two temperatures, and one minor peak emerges at 44.4 ° that cannot be assigned to the monoclinic phase. By 130 °C, the material has completely transformed, and the peaks can be fully indexed to a simple cubic pattern with lattice parameter a=4.989(1) Å.

The similarity of the pattern at 130 °C to that of cubic CsH<sub>2</sub>PO<sub>4</sub>[21] (space group  $Pm\bar{3}m$ ) motivated Rietveld refinement using the phosphate structure as the initial model. The P atom of the phosphate was replaced with Se and P with fixed 0.5 occupancy each and identical displacement parameters. The lattice parameter, the isotropic displacement factors of Cs and Se/P, and the position of O were allowed to vary (Cs and Se/P reside on the fixed 1a and 1b special positions, respectively). The oxygen displacement parameter was treated as isotropic and was fixed to a value  $1.07\times$  that of the Se/P atom, in analogy to the relative values of the displacement factors of O and P in CsH<sub>2</sub>PO<sub>4</sub>.[21] The final refinement, Figure 2(a), resulted in good agreement between the model and the data, with refinement statistics of  $R_{wp} = 9.81\%$ ,  $R_{bragg} = R_F = 5.87\%$ , and GooF = 3.56. The final crystallographic parameters are reported in Table 1.

As with cubic  $CsH_2PO_4[21]$  and cubic  $Cs_2(HSO_4)(H_2PO_4)[11]$ , the single, crystallographically unique oxygen atom in cubic  $Cs_2(HSeO_4)(H_2PO_4)$  resides in a 24l site with 1/6 occupancy, suggesting at least six orientations of the tetrahedral  $XO_4$  group. The refined oxygen position (Table 1) results in an X-O bond length of 1.59(6) Å, an intermediate value between those typical of P-O bonds,[22] which range at room temperature from 1.49 Å to 1.59 Å, and Se-O bonds,[23] which fall between 1.601(3) Å and 1.715(3) Å at room temperature. Analysis of the full suite of diffraction patterns revealed that the thermal expansion is linear over the range from 130 to 220 °C, Figure 2(b), with a linear thermal expansion coefficient of  $\alpha_L = 1.05(3) \times 10^{-4}/K$ . This is more than twice the thermal expansion coefficient of  $CsH_2PO_4$ , of  $3.92(11) \times 10^{-5}$  [24], suggesting a dominant role of the X-O bonds in the thermal expansivity. At 220 °C the cell parameter of  $Cs_2(HSeO_4)(H_2PO_4)$  is 5.0353(9) Å. This is substantially larger than that of  $CsH_2PO_4$ , 4.9673(9) Å at 230 °C[24], the temperature at which the phosphate superprotonic phase is first encountered on heating. This reflects again the larger X-O bond lengths in the selenate. At 145 °C, the cell parameter of  $Cs_2(HSeO_4)(H_2PO_4)$ , 4.9974(4) Å, is surprisingly similar to that of  $Cs_2(HSO_4)(H_2PO_4)$ , 4.926(6) Å (at the same temperature)[25].

The conductivity (Figure 3) and STA (Figure 4) profiles of Cs<sub>2</sub>(HSeO<sub>4</sub>)(H<sub>2</sub>PO<sub>4</sub>), under similar light humidification conditions of those of the XRD measurements (pH<sub>2</sub>O = 0.05 atm), reveal the occurrence of a superprotonic transition. Representative impedance spectra, for the low and high temperature behavior, are shown in Figure S1. The result is generally consistent with the findings of Zouari et al.[18] and is entirely consistent with the finding here of a cubic, disordered structure in the high temperature phase. Between 120 °C and 130 °C the conductivity, Figure 3, rises by about a factor of 30 and approaches a value of  $10^{-2}$  S/cm at the maximum measurement temperature of 217 °C. The thermal analysis, Figure 4, shows the transition to initiate at 116 °C and to be distinct from mass loss events. Integration of the DSC peak yielded a heat of transition of 40.9 J/g. Notably, Zouari et al.[18] report thermal stability of Cs<sub>2</sub>(HSeO<sub>4</sub>)(H<sub>2</sub>PO<sub>4</sub>) under presumably dry conditions up to a temperature of 198 °C, whereas in the present study, mass loss initiates under dry conditions at 119 °C (Figure S3a). It is likely the difference results from the higher heating rate used in the earlier work (10 °C/min) in contrast to 1 °C/min used here; as heating rates increase, thermal events are detected at increasingly higher temperatures. In sum, while there are minor differences with the prior work, the XRD,

conductivity, and STA measurements are all in agreement that the material transforms to a cubic, superprotonic phase, with the transition occurring broadly over the range from 116 to 130 °C.

In the superprotonic state,  $Cs_2(HSeO_4)(H_2PO_4)$  was found to be easily deformed. Due to the significant softening at high temperature, the sample dimensions before and after measurement were noticeably different, introducing uncertainty in the conversion from measured resistance to conductivity. The error bars shown in Figure 3 reflect the evolution of sample dimensions over the course of the measurement. Moreover, there was a detectable difference between the conductivity of the superprotonic phase as recorded on heating and on cooling (amounting to about 25% at ~ 145 °C). Because of possible reaction with steam on cooling (see discussion below), we consider the data collected on heating to be the more reliable dataset. Using these data, the conductivity in the superprotonic phase was described according to  $\sigma = \frac{A}{T} \exp\left(-E_a/k_bT\right)$  to obtain the activation energy,  $E_a$  (= 0.304 ± 0.002 eV), and the preexponential factor, A [log (A/S·cm<sup>-1</sup>K) = 3.80 ± 0.02].

Beyond confirmation of a superprotonic transition, the results in Figure 3 show that the conductivity of superprotonic Cs<sub>2</sub>(HSeO<sub>4</sub>)(H<sub>2</sub>PO<sub>4</sub>) measured here is about an order of magnitude larger than that reported by Zouari et al.[18], and is similar to the two prior reports for Cs<sub>2</sub>(HSO<sub>4</sub>)(H<sub>2</sub>PO<sub>4</sub>).[11, 19] Moreover, extrapolation to 250 °C suggests a conductivity of 1.45 × 10<sup>-2</sup> S/cm, comparable to that of CsH<sub>2</sub>PO<sub>4</sub> at this same temperature [26]. Thus, Cs<sub>2</sub>(HSeO<sub>4</sub>)(H<sub>2</sub>PO<sub>4</sub>) does not have an anomalously low conductivity in its cubic phase. The impact of replacing S with Se is limited to inducing a slight decrease in both activation energy and pre-exponential factor, Table 2. The only other example in which selenate and sulfate solid acids are isostructural in their superprotonic phase is tetragonal CsHSeO<sub>4</sub>/CsHSO<sub>4</sub>. Literature disagreements make determination of the role of the anion difficult in this case also. Nevertheless, the preponderance of the evidence (Figure S2) indicates that the selenate[3] and sulfate[4] [27] analogs have very similar conductivities in the Scheelite structure-type as well. The low activation energy for proton transport in Cs<sub>2</sub>(HSeO<sub>4</sub>)(H<sub>2</sub>PO<sub>4</sub>) relative to that of CsH<sub>2</sub>PO<sub>4</sub> supports the conclusion of Yamane et al.[19] (who studied the cubic solid solution region between CsH<sub>2</sub>PO<sub>4</sub> and CsHSO<sub>4</sub>) that decreasing the number of hydrogen bonds in the cubic superprotonic phase decreases the activation energy for polyanion group reorientation, the rate-limiting step in the long-range transport in the phosphate end-member.

A minor distinction between  $Cs_2(HSeO_4)(H_2PO_4)$  and the related solid acid materials is the somewhat diffuse change in conductivity at the transition, which is accompanied by a broad thermal event, spanning ~25 °C in the DSC profile. The reason for this is unknown. Interestingly, Zouari et al.[18] report a similarly broad thermal event in their DTA measurements, but a sharper change in conductivity at the transition, a feature which is due in part to the larger steps in the conductivity measurement (10 °C in that work vs. 5 °C here).  $Cs_2(HSeO_4)(H_2PO_4)$  is also distinct in that the overall increase in conductivity across the transition is modest, reflecting the already high conductivity in the monoclinic phase.

The thermal properties of the superprotonic transition of Cs<sub>2</sub>(HSeO<sub>4</sub>)(H<sub>2</sub>PO<sub>4</sub>) merit some discussion. The average value of the enthalpy of transition,  $\Delta H_{trans}$ , from the measurements under 0.05 (Figure 4) and 0.04 atm (Figure S3), under which conditions the profiles were not impacted by drift during humidity stabilization, is 40 J/g, or 18 kJ/mol (determined from the area under the DSC anomaly). The breadth of the DSC anomaly might be considered to reflect a second order transition, however, the significant change in structure between monoclinic and cubic phases (for example, there are four formula units per unit cell in the monoclinic structure and only one in the cubic, and the anions sit in distinct sites in the monoclinic phase but are randomly arranged on a single site in the cubic phase) argues against this. Regardless of the order of the transition, its entropy,  $\Delta S_{trans}$ , can be estimated according to  $\Delta S_{trans} = \frac{\Delta H_{trans}}{T_{trans}}$ where  $T_{trans}$  is the transition temperature, defined by the onset of the thermal event. Significantly, the transition entropies per mole XO<sub>4</sub> unit across Cs<sub>2</sub>(HSeO<sub>4</sub>)(H<sub>2</sub>PO<sub>4</sub>), Cs<sub>2</sub>(HSO<sub>4</sub>)(H<sub>2</sub>PO<sub>4</sub>), and CsH<sub>2</sub>PO<sub>4</sub> are all approximately 23 J/mol-K. This suggests that the configurational entropy in the high temperature phase dominates the transition entropy, with little influence of the distinct room temperature structures adopted by Cs<sub>2</sub>(HSeO<sub>4</sub>)(H<sub>2</sub>PO<sub>4</sub>), Cs<sub>2</sub>(HSO<sub>4</sub>)(H<sub>2</sub>PO<sub>4</sub>), and CsH<sub>2</sub>PO<sub>4</sub> in establishing the difference in entropies between the room temperature and superprotonic phases. In addition, the transition temperatures of Cs<sub>2</sub>(HSeO<sub>4</sub>)(H<sub>2</sub>PO<sub>4</sub>) and Cs<sub>2</sub>(HSO<sub>4</sub>)(H<sub>2</sub>PO<sub>4</sub>) differ by only approximately 40 °C, Table 2, reflecting the 10% difference in transition enthalpies between these two materials.

Changes in the humidification level induced significant changes in the transition behavior of  $Cs_2(HSeO_4)(H_2PO_4)$ . In general, increasing  $pH_2O$  levels suppressed the mass loss to higher temperatures, Figure 5, suggesting that the mass change is largely due to  $H_2O$  release as opposed to loss of  $SeO_x$  or  $PO_x$  species. However, increasing the steam partial pressure from 0.2 to 0.4

atm enhanced the rate of the initial gradual mass loss, contrary to typical behavior. While initial mass losses are often associated with desorption from surfaces, the present set of curves do not show a plateau region that would normally follow surface dehydration and precede bulk mass loss, and thus the data preclude ready differentiation between these two types of responses. The second thermal event in the DSC profile (example shown in Figure 4 and complete set of profiles presented in Figure S3) can be plausibly attributed to bulk mass loss given its alignment in all cases with a large peak in the differential mass loss (dTG) plots. This major event clearly shifts to higher temperature with increasing  $pH_2O$ .

Beyond suppressing major mass loss, exposure to high humidification levels ( $pH_2O = 0.3$ atm) led to distinct changes in the high temperature phase evolution, Figure 6. Most significant was the appearance of a secondary phase, as evidenced by peaks at 24.8 and 28  $^{\circ}$  2 $\Theta$ . Furthermore, the monoclinic phase, which disappeared under low pH<sub>2</sub>O by 130 °C (Figure 1), remained present in the pattern collected at this temperature under high pH<sub>2</sub>O. At 150 °C and higher, the patterns under  $pH_2O = 0.3$  atm are dominated by the cubic superprotonic phase, and the additional minor peaks are clearly resolvable. These peaks could be indexed to a trigonal unit cell, with lattice parameters (a = 6.346(5) Å, c = 23.54(1) Å at 110 °C) similar to those of  $Cs_3H(SeO_4)_2$  in its superprotonic phase (a = 6.4260(6), c = 23.447(2) at 197 °C[28]). However, trigonal Cs<sub>3</sub>H(SeO<sub>4</sub>)<sub>2</sub> occurs at a transition temperature of 183 °C[28] and is not expected at 110 °C. Its detection at such a low temperature immediately indicates that the trigonal phase encountered here is chemically distinct from Cs<sub>3</sub>H(SeO<sub>4</sub>)<sub>2</sub>. The result also implies that the cubic phase in these patterns is chemically distinct from Cs<sub>2</sub>(HSeO<sub>4</sub>)(H<sub>2</sub>PO<sub>4</sub>). With the phases broadly identified, the patterns were analyzed by Rietveld refinement using simplified compositions of CsH<sub>2</sub>PO<sub>4</sub> for the cubic phase and Cs<sub>3</sub>H(SeO<sub>4</sub>)<sub>2</sub> for the trigonal phase, while retaining the composition of Cs<sub>2</sub>(HSeO<sub>4</sub>)(H<sub>2</sub>PO<sub>4</sub>) for the monoclinic phase. Good agreement was obtained between the structural model and the data (Figure S4), indicating the suitability of the model. The results of the refinements (weight fraction of the phases, lattice parameter of the cubic phase, and cell volume of the trigonal phase) are summarized in Figure 7. The behavior is reminiscent of Cs<sub>3</sub>H<sub>3</sub>(PO<sub>4</sub>)<sub>2</sub>, which exsolves a small amount of a CsH<sub>2</sub>PO<sub>4</sub>-like cubic phase at temperatures below the superprotonic transition of conventional CsH<sub>2</sub>PO<sub>4</sub>.[29]

While a comprehensive study of the phase behavior of Cs<sub>2</sub>(HSeO<sub>4</sub>)(H<sub>2</sub>PO<sub>4</sub>) under high steam conditions is beyond the scope of this work, a possible explanation for the observed

behavior is that the presence of steam induces evaporation of selenic acid. Loss of H<sub>2</sub>SeO<sub>4</sub> would leave behind a solid that is rich in CsH<sub>2</sub>PO<sub>4</sub> and Cs<sub>3</sub>H(SeO<sub>4</sub>)<sub>2</sub> relative to the original composition promoting the formation of a phosphate-rich cubic phase and a phosphate-doped trigonal phase. The cell parameters of the cubic phase in the presence of the trigonal phase are smaller than those of cubic stoichiometric Cs<sub>2</sub>(HSeO<sub>4</sub>)(H<sub>2</sub>PO<sub>4</sub>), Figure 7b, consistent with phosphate enrichment, while the occurrence of this cubic phase at temperatures below 230 °C indicates it must be chemically distinct from CsH<sub>2</sub>PO<sub>4</sub>. Similarly, the cell volume of the trigonal phase is significantly smaller than that of stoichiometric Cs<sub>3</sub>H(SeO<sub>4</sub>)<sub>2</sub>, Figure 7c (lattice parameters are reported in Figure S5). To the authors' knowledge, no study has to date examined phosphate doping of Cs<sub>3</sub>H(SeO<sub>4</sub>)<sub>2</sub> or analogs. However, the Cs<sub>3</sub>H<sub>3</sub>(PO<sub>4</sub>)<sub>2</sub> has a pseudo-trigonal structure similar to that of Cs<sub>3</sub>H(SeO<sub>4</sub>)<sub>2</sub>.[29] Given the miscibility of CsHSeO<sub>4</sub> and CsH<sub>2</sub>PO<sub>4</sub> at high temperature, high temperature miscibility between Cs<sub>3</sub>H(SeO<sub>4</sub>)<sub>2</sub> and Cs<sub>3</sub>H<sub>3</sub>(PO<sub>4</sub>)<sub>2</sub>, resulting in a depression of the transition temperature to the trigonal phase, is highly plausible. Furthermore, the decrease in cell volume relative to stoichiometric Cs<sub>3</sub>H(SeO<sub>4</sub>)<sub>2</sub> is consistent with phosphate doping. The hypothesis that steam induces evaporation of selenic acid could also explain the surprising result that at 250 °C, the mass under 0.4 atm is less than that under 0.2 atm, Figure 5. However, to attain a trigonal phase that amounts to  $\sim 15\%$  of the sample mass by weight as observed from the X-ray refinement at 150 °C, approximately 3% mass loss due to selenic acid evaporation would be required, far greater than the  $\sim 0.015\%$  observed at this temperature in the TGA experiments, Figure 4. The discrepancy could arise from the differences in gas flow dynamics between the two experiments, with greater gas access to the solid in the XRD study, or from the effectively lower heating rate used in the XRD experiments (after accounting for equilibration and data acquisition time at each measurement temperature).

An alternative explanation is that a  $Cs_3H_x(XO_4)_2$  phase simply exsolves from the parent cubic phase, leaving the latter deficient in Cs relative to the anion content and with charge balance provided by the presence of excess protons. The fact that cubic  $Cs_{1-x}H_{2+x}PO_4$  is known[30] supports this hypothesis. However, Cs deficiency in  $Cs_{1-x}H_{2+x}PO_4$  results in lattice expansion rather than the contraction observed here (Figure 7b). Moreover, the connection to gas phase composition is not obvious for a solid state exsolution process. Complete unraveling of this mystery awaits future study.

### **Summary and Conclusions**

The compound Cs<sub>2</sub>(HSeO<sub>4</sub>)(H<sub>2</sub>PO<sub>4</sub>) undergoes a superprotonic transition to a cubic phase that initiates at approximately 116 °C. The transition is somewhat more gradual than observed in analogous superprotonic materials, with its completion occurring at approximately 130 °C. The onset of this broad transition is reported here as the transition temperature. The rise in conductivity across the transition is moderate, about a factor of thirty, a feature reflecting the high conductivity in the low temperature phase. In the cubic phase, the activation energy for proton transport is 0.304(2) eV, and the conductivity is comparable to that of Cs<sub>2</sub>(HSO<sub>4</sub>)(H<sub>2</sub>PO<sub>4</sub>). Replacing S with Se in the cubic phase has negligible impact on the transport properties, whereas it causes a slight increase in the transition temperature from the monoclinic phase. Despite differences in the room temperature structures of Cs<sub>2</sub>(HSeO<sub>4</sub>)(H<sub>2</sub>PO<sub>4</sub>), Cs<sub>2</sub>(HSO<sub>4</sub>)(H<sub>2</sub>PO<sub>4</sub>) and CsH<sub>2</sub>PO<sub>4</sub>, they each display monoclinic to cubic transformation entropy of approximately 23 J/mol(CsH<sub>x</sub>XO<sub>4</sub>)-K. Under  $pH_2O = 0.05$  atm. Moreover, the cubic phase of Cs<sub>2</sub>(HSeO<sub>4</sub>)(H<sub>2</sub>PO<sub>4</sub>) is stable to approximately 250 °C, although some of this stabilization is likely due to kinetic effects of a finite heating rate. Establishing thermodynamic stability limits requires extrapolation to zero heating rate[26] or prolonged isothermal holds[31]. Under elevated pH<sub>2</sub>O (0.3 atm), exsolution of a trigonal phase, with structure analogous to that of Cs<sub>3</sub>H(SeO<sub>4</sub>)<sub>2</sub>, was found to accompany the transformation to the cubic phase. This transformation is tentatively attributed to evaporation of H<sub>2</sub>SeO<sub>4</sub>, leaving behind a solid that is rich in CsH<sub>2</sub>PO<sub>4</sub> and Cs<sub>3</sub>H(SeO<sub>4</sub>)<sub>2</sub> relative to the starting composition, though simple exsolution of a trigonal phase, leaving the cubic phase rich in cation vacancies, cannot be ruled out. Regardless of the specific mechanism, observation of the trigonal phase at temperatures below the superprotonic transition of stoichiometric Cs<sub>3</sub>H(SeO<sub>4</sub>)<sub>2</sub> suggests that phosphate doping may stabilize M<sub>3</sub>H(SeO<sub>4</sub>)<sub>2</sub> and M<sub>3</sub>H(SO<sub>4</sub>)<sub>2</sub> phases at temperatures below those at which their respective stoichiometric superprotonic transitions occur.

### CRediT authorship contribution statement

Grace Xiong – Conceptualization, Investigation, Formal Analysis, Writing – original draft; Ara Jo – Conceptualization, Investigation, Writing – review and editing; Louis S. Wang –

Methodology, Writing – review and editing; Sossina M. Haile – Conceptualization, Supervision, Funding acquisition, Writing – review and editing

## Declaration of competing interests

The authors declare that they have no competing financial interests or personal relationships that have influenced the work reported in this paper.

## Data availability

Data will be made available on request.

# Acknowledgments

Financial support has been provided by the National Science Foundation (DMR-1807234, OAC-2118201, and DGE-1842165). This work made use of the J.B. Cohen X-Ray Diffraction facility at Northwestern University, supported by the NSF MRSEC program (NSF DMR- 2308691). We thank Elise Goldfine for assistance with diffraction measurements.

### **Tables**

Table 1. Crystallographic refinement of the cubic  $Cs_2(HSeO_4)(H_2PO_4)$  phase at T = 130 °C with space group  $Pm\overline{3}m$  and lattice constant a = 4.989(1) Å.

Atom	х	У	Z	site	occupancy	Uiso (Ų)
Cs	0	0	0	1 <i>a</i>	1	0.109(4)
Se/P	0.5	0.5	0.5	1 <i>b</i>	0.5/0.5	0.065(5)
O	0.5	0.207(4)	0.386(6)	24 <i>l</i>	0.167	$0.069(5)^1$

<sup>1.</sup> constrained Uiso of oxygen to be 1.07x Se/P Uiso.

Table 2. Proton transport and phase transformation properties of  $Cs_2(HSeO_4)(H_2PO_4)$  and selected related materials.

Compound	E <sub>a</sub> , eV	log(A / S.cm <sup>-1</sup> K)	Source	Tsp °C	ΔH J/g	ΔS <sup>a</sup> J/mol-K	Source
Cs <sub>2</sub> (HSeO <sub>4</sub> )(H <sub>2</sub> PO <sub>4</sub> )	0.304(2)	3.80(2)	this work	116	40	23	this work
$Cs_2(HSeO_4)(H_2PO_4)$	0.24	N/A	Zouari [18]	127 <sup>b</sup>	N/A	N/A	Zouari[18]
$Cs_2(HSO_4)(H_2PO_4)$	0.37(1)	4.8(1)	Chisholm[11]	65°	44	23.5	Chisholm[17]
$Cs_2(HSO_4)(H_2PO_4)$	0.354(1)	4.18(2)	Yamane[19]	97°	45	26.4	Takahashi[25]
$CsH_2PO_4$	$0.398(1)^d$	$4.91(1)^d$	Ikeda[24]	230	50.9	23.3	Ikeda[24]
$CsH_2PO_4$	0.418(2)	5.19(2)	Haile[1]	228	49.0	22.6	Boysen[26]

<sup>(</sup>a) per mole XO<sub>4</sub> unit

<sup>(</sup>b) peak rather than onset; onset is relatively close to the value of 116 °C (onset) obtained in the present work.

<sup>(</sup>c) peak rather than onset

<sup>(</sup>d) Two typographical errors in the work of Ikeda *et al.*[24] are corrected here: (1) the units for activation energy were reported to be in eV, but the units employed were in fact kJ/mol; (2) the pre-exponential term was stated to correspond to log(A), but in fact the reported value corresponds to ln(A).

### **Figures**

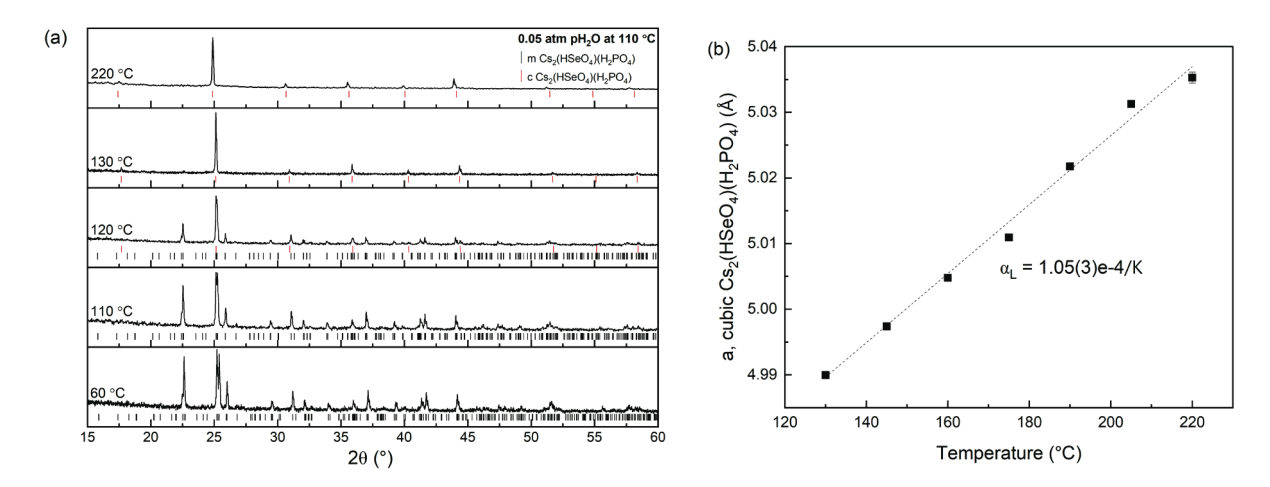


Figure 1. In situ X-ray diffraction study of  $Cs_2(HSeO_4)(H_2PO_4)$  under 0.05 atm pH<sub>2</sub>O (balance  $N_2$ ): (a) diffraction patterns at the temperatures indicated (the measurement at 60 °C was carried out under dry  $N_2$ ); (b) lattice parameter as a function of temperature of the cubic phase that forms at high temperature. By 130 °C, the material has fully transitioned to the cubic phase, which is stable to at least 220 °C.

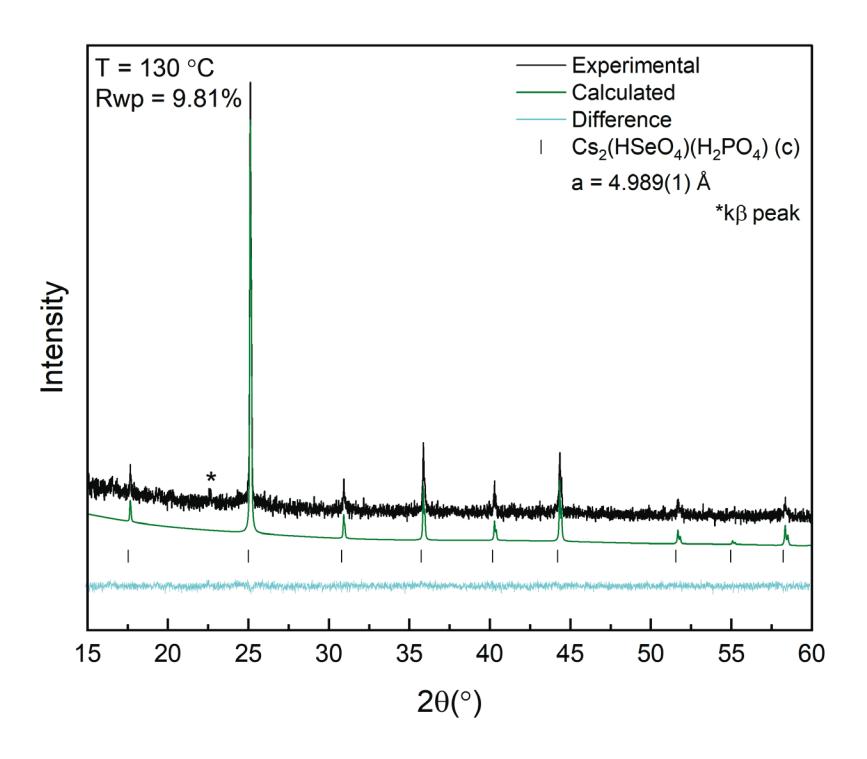


Figure 2. Rietveld refinement of cubic  $Cs_2(HSeO_4)(H_2PO_4)$  phase at the representative temperature of 130 °C ( $pH_2O = 0.05$  atm, balance  $N_2$ ). The peak at 22.6 °2  $\theta$  is taken to be the  $k\beta$  satellite [ $\lambda(Cu_k\beta) = 1.392$  Å] of the (110) cubic peak at 25.1 °2  $\theta$  due to its position and relative intensity, and the absence of any other minor peaks with intensity above the noise level.

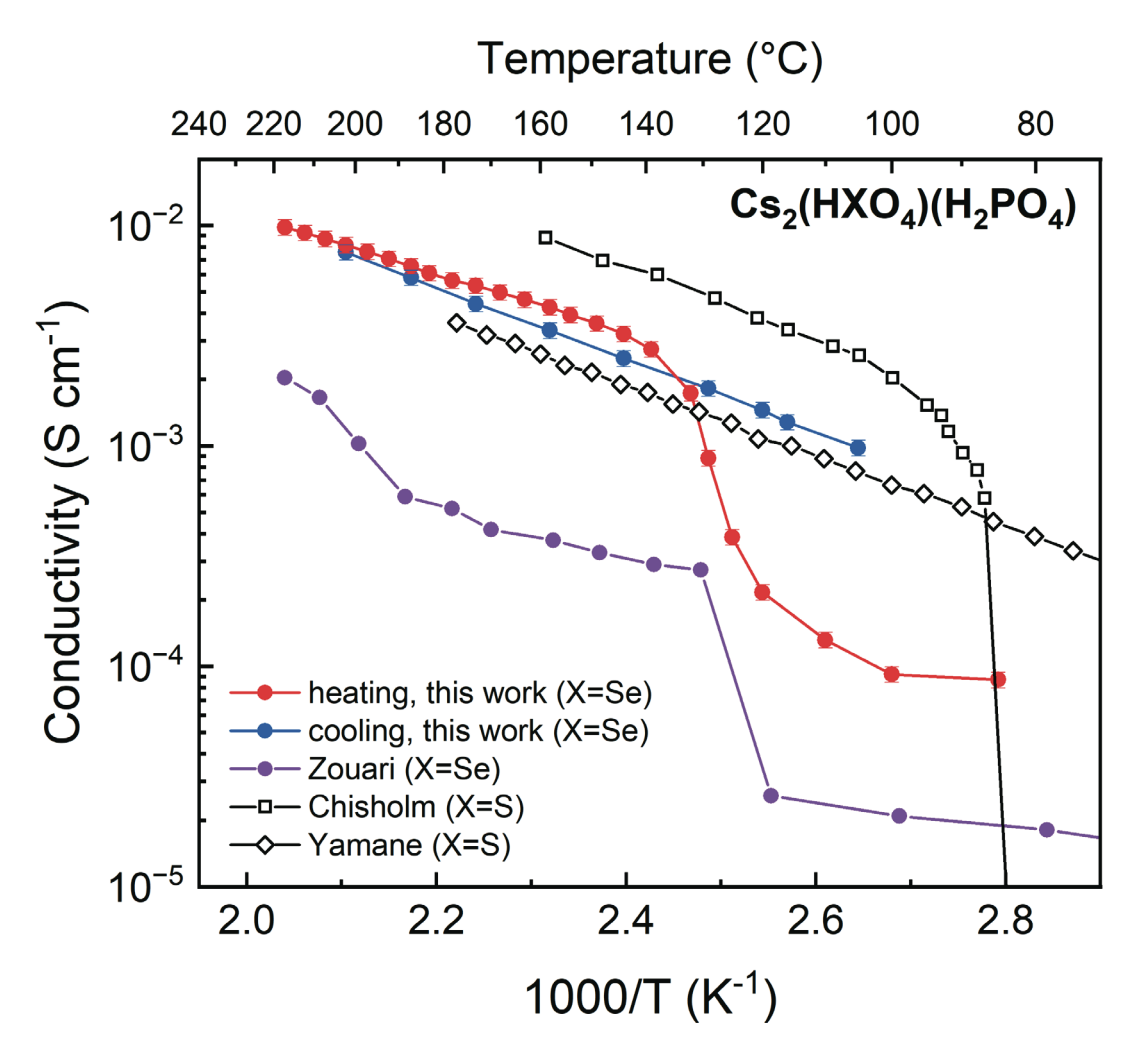


Figure 3. Temperature dependence of the conductivity of  $Cs_2(HSeO_4)(H_2PO_4)$  measured here and compared to a previous report of this material [18] and two reports of the related compound  $Cs_2(HSO_4)(H_2PO_4)[11, 19]$ . Measurements of  $Cs_2(HSeO_4)(H_2PO_4)$  in this work were made under  $pH_2O = 0.05$  atm (balance  $N_2$ ), except for temperatures of 110 °C and lower, at which the atmosphere was dry  $N_2$ .

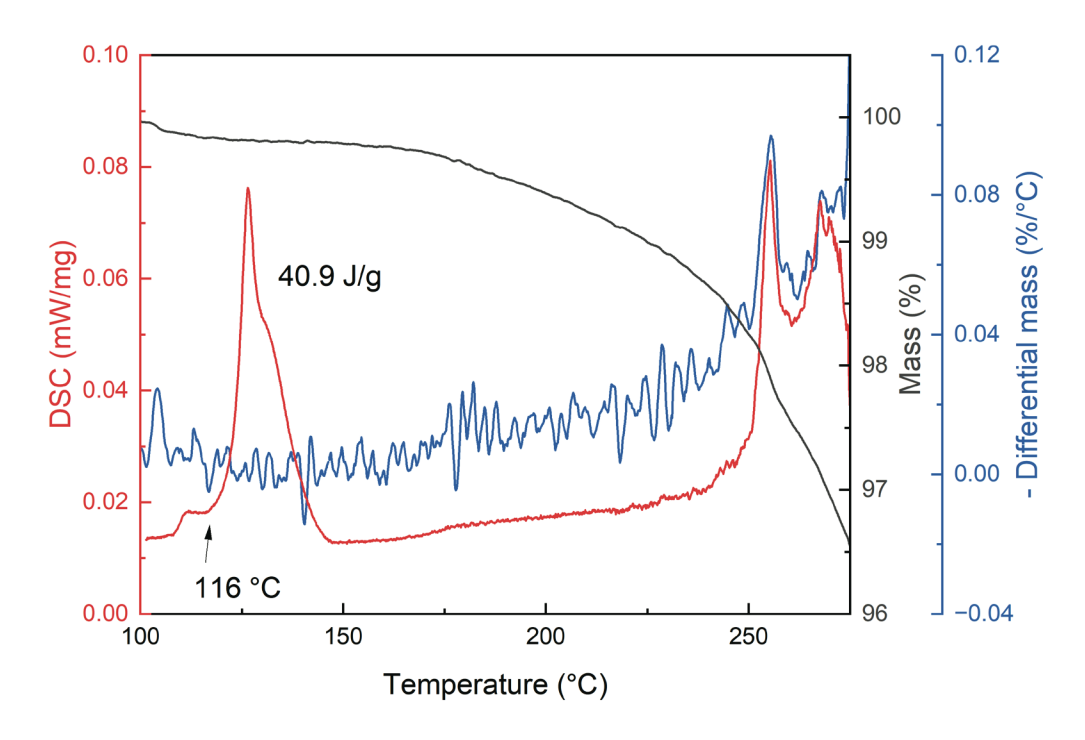


Figure 4. Thermal analysis of  $Cs_2(HSeO_4)(H_2PO_4)$ : simultaneous TG and DSC profiles collected under 0.05 atm pH<sub>2</sub>O (balance Ar). The large thermal event that initiates at ~ 116 °C corresponds to the superprotonic transition to the cubic phase.

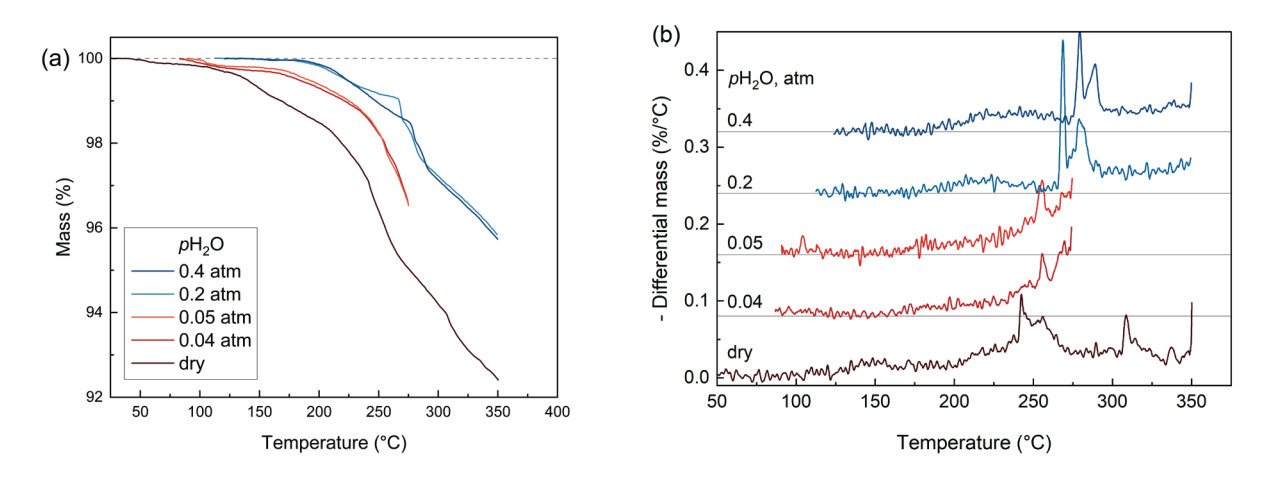


Figure 5. (a) Mass loss profiles of  $Cs_2(HSeO_4)(H_2PO_4)$  under different steam partial pressures as indicated. The relative mass following the initial equilibration in the atmosphere of interest is set to 100%; some of the mass may be due to surface adsorbed  $H_2O$ . (b) Differential mass profiles, offset for clarity (with zero value as indicated by the additional horizontal lines).

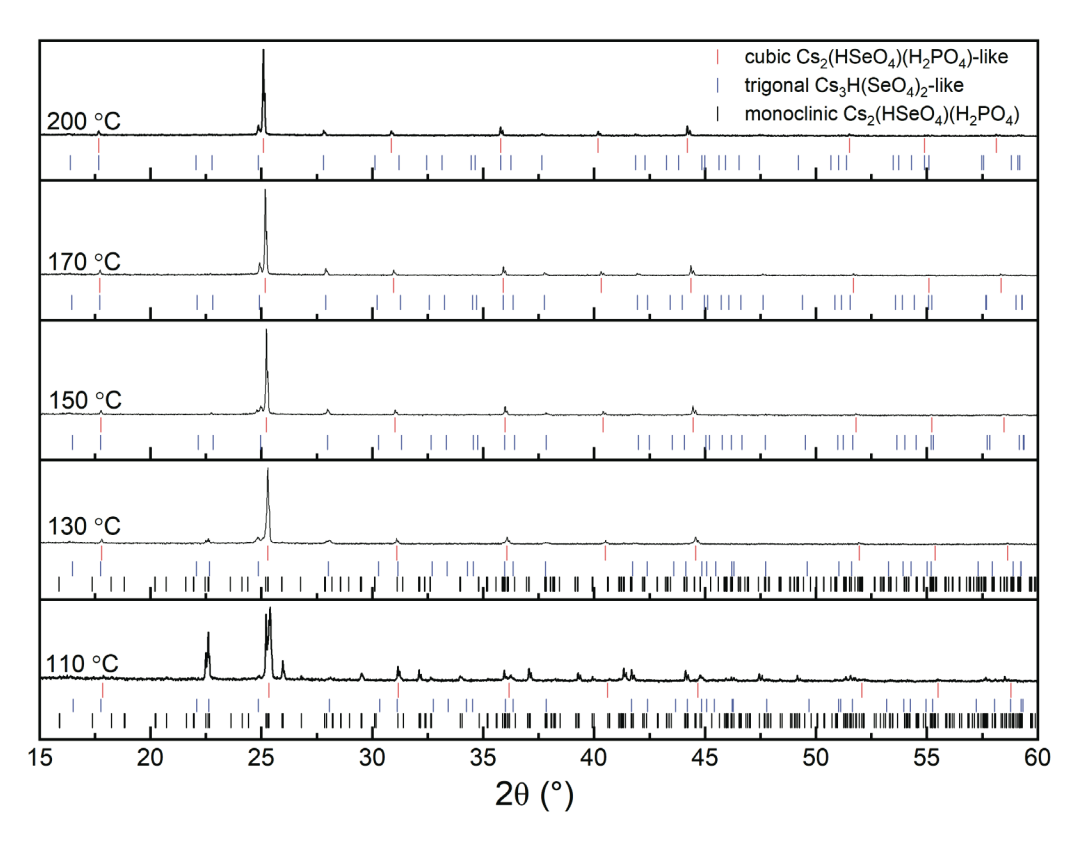


Figure 6. In situ X-ray diffraction study of  $Cs_2(HSeO_4)(H_2PO_4)$  under 0.3 atm pH<sub>2</sub>O (balance  $N_2$ ). Patterns measured at temperatures indicated.

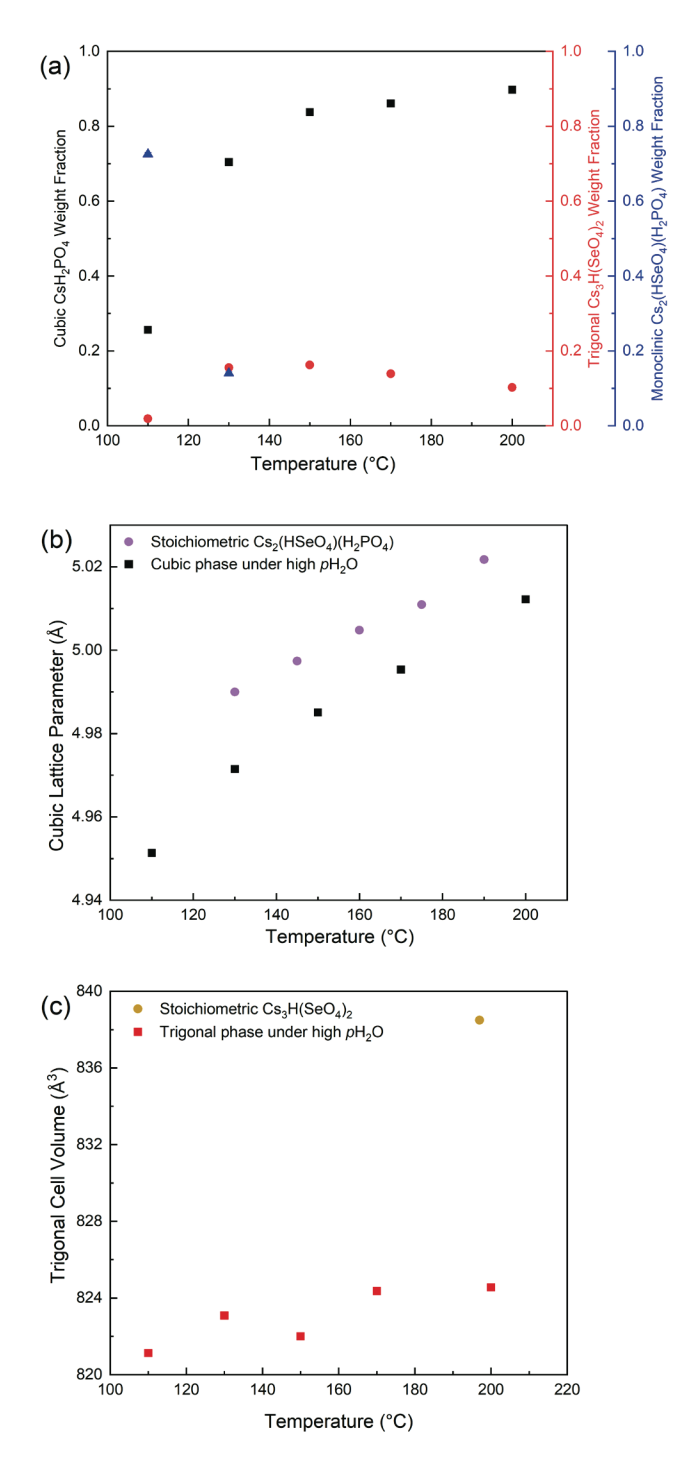


Figure 7. Results of Rietveld analysis of the phase evolution of  $Cs_2(HSeO_4)(H_2PO_4)$  under 0.3 atm: (a) weight fractions of phases; (b) lattice parameter of the observed cubic phase, and (c) the cell volume of the trigonal phase. For simplicity and in the absence of detailed compositional information, analysis was performed assuming stoichiometric chemical formulae as indicated in (a). In (b) the lattice parameter of stoichiometric cubic  $Cs_2(HSeO_4)(H_2PO_4)$  (Figure 1) is shown for comparison. In (c) the cell volume of stoichiometric trigonal  $Cs_3H(SeO_4)_2$  is shown for comparison[28].

### References

- [1] S.M. Haile, C.R.I. Chisholm, K. Sasaki, D.A. Boysen, T. Uda, *Faraday Discussions* **134** (2007) 17.
- [2] A.I. Baranov, V.P. Khiznichenko, V.A. Sandler, L.A. Shuvalov, *Ferroelectrics* **81** (1988) 1147.
- [3] A. Baranov, L. Shuvalov, N. Shchagina, *JETP Letters* **36** (1982) (11) 459.
- [4] T. Norby, M. Friesel, B.E. Mallander, *Solid State Ionics* **77** (1995) 105.
- [5] C.R.I. Chisholm, Y.H. Jang, S.M. Haile, W.A. Goddard, *Physical Review B* 72 (2005) (13).
- [6] B.V. Merinov, S.M. Haile, U. Bismayer, Solid State Ionics 146 (2002) (3-4) 355.
- [7] A. Pawlowski, C. Pawlaczyk, B. Hilczer, Solid State Ionics 44 (1990) (1-2) 17.
- [8] D.Z. Yi, S. Sanghvi, C.P. Kowalski, S.M. Haile, *Chemistry of Materials* **31** (2019) (23) 9807.
- [9] S.M. Haile, K.D. Kreuer, J. Maier, *Acta Crystallographica Section B-Structural Science* **51** (1995) 680.
- [10] S.M. Haile, G. Lentz, K.-D. Kreuer, J. Maier, *Solid State Ionics* **77** (1995) 128.
- [11] C.R.I. Chisholm, S.M. Haile, *Solid State Ionics* **136-137** (2000) 229.
- [12] C.R.I. Chisholm, Superprotonic Phase Transitions in Solid Acids: Parameters affecting the presence and stability of superprotonic transitions in the MH<sub>n</sub>XO<sub>4</sub> family of compounds (X=S, Se, P, As; M=Li, Na, K, NH<sub>4</sub>, Rb, Cs), *Materials Science*, California Institute of Technology, Pasadena (2003).
- [13] V.V. Grebenev, I.P. Makarova, D.A. Ksenofontov, V.A. Komornikov, E.V. Dmitricheva, *Crystallography Reports* **58** (2013) (6) 894.
- [14] M.A. Zakharov, S.I. Troyanov, E. Kemnitz, *Zeitschrift für Kristallographie Crystalline Materials* **216** (2001) (3) 172.
- [15] A.S. Mikheykin, D.Y. Chernyshov, I.P. Makarova, V.V. Grebenev, V.A. Komornikov, E.V. Selezneva, *Solid State Ionics* **305** (2017) 30.
- [16] A. Baranov, Crystallography Reports **48** (2003) (6) 1012.
- [17] C.R.I. Chisholm, S.M. Haile, *Acta Crystallographica Section B-Structural Science* **55** (1999) 937.
- [18] N. Zouari, K. Jaouadi, T. Mhiri, A. Daoud, E. Lebraud, P. Gravereau, *Journal of Molecular Structure* **842** (2007) (1) 81.
- [19] Y. Yamane, K. Yamada, K. Inoue, Solid State Ionics 179 (2008) (13) 483.
- [20] B.H. Toby, R.B. Von Dreele, Journal of Applied Crystallography 46 (2013) (2) 544.
- [21] K. Yamada, T. Sagara, Y. Yamane, H. Ohki, T. Okuda, Solid State Ionics 175 (2004) (1) 557.
- [22] M. Ichikawa, Acta Crystallographica Section B 43 (1987) (1) 23.
- [23] T. Fukami, R.H. Chen, *Physica Status Solidi* (a) **199** (2003) 378.
- [24] A. Ikeda, D.A. Kitchaev, S.M. Haile, Journal of Materials Chemistry A 2 (2014) (1) 204.
- [25] H. Takahashi, Y. Suzuki, T. Sakuma, Solid State Ionics 285 (2016) 155.
- [26] D.A. Boysen, S.M. Haile, H. Liu, R.A. Secco, *Chemistry of Materials* **15** (2003) (3) 727.
- [27] D.A. Boysen, Superprotonic Solid Acids: Structure, Properties, and Applications, *Materials Science and Engineering*, California Institute of Technology (2004).
- [28] B.V. Merinov, A.I. Baranov, L.A. Shuvalov, *Kristallografiya* **35** (1990) (2) 355.
- [29] S. Sanghvi, S.M. Haile, Journal of Solid State Chemistry 296 (2021).

- [30] L.S. Wang, S.V. Patel, E. Truong, Y.-Y. Hu, S.M. Haile, *Chemistry of Materials* **34** (2022) (4) 1809.
- [31] A. Ikeda, S.M. Haile, Solid State Ionics **213** (2012) 63.